Calcium-Modulated S100 Protein−Phospholipid Interactions. An NMR Study of Calbindin D_{9k} and DPC†

Anders Malmendal,*,‡,§ Craig W. Vander Kooi,‡ Niels Chr. Nielsen,§ and Walter J. Chazin*,‡

Departments of Biochemistry and Physics, Center for Structural Biology, 5140 BIOSCI/MRB III, Vanderbilt University, Nashville, Tennessee 37232-8725, and Center for Insoluble Protein Structures (inSPIN) and Interdisciplinary Nanoscience Center (iNANO), Department of Chemistry, University of Aarhus, DK-8000 Aarhus C, Denmark

Received January 14, 2005; Revised Manuscript Received March 15, 2005

ABSTRACT: The cellular functions of several S100 proteins involve specific interactions with phospholipids and the cell membrane. The interactions between calbindin D_{9k} (S100D) and the detergent dodecyl phosphocholine (DPC) were studied using NMR spectroscopy. In the absence of Ca^{2+}, the protein associates with DPC micelles. The micelle-associated state has intact helical secondary structures but no apparent tertiary fold. At neutral pH, Ca^{2+}-loaded calbindin D_{9k} does not associate with DPC micelles. However, a specific interaction is observed with individual DPC molecules at a site close to the linker between the two EF-hands. Binding to this site occurs only when Ca^{2+} is bound to the protein. A reduction in pH in the absence of Ca^{2+} increases the stability of the micelle-associated state. This along with the corresponding reduction in Ca^{2+} affinity causes a transition to the micelle-associated state also in the presence of Ca^{2+} when the pH is lowered. Site-specific analysis of the data indicates that calbindin D_{9k} has a core of three tightly packed helices (A, B, and D), with a dynamic fourth helix (C) more loosely associated. Evidence is presented that the Ca^{2+}-binding characteristics of the two EF-hands are distinctly different in a micelle environment. The role of calbindin D_{9k} in the cell is discussed, along with the broader implications for the function of the S100 protein family.

A number of well-characterized proteins have been shown to exist in dynamic exchange between cytosolic and membrane-associated states, regulated by specific cellular signals. Understanding the function and interactions of these proteins in a cellular environment requires consideration of the laws governing these interactions and the structural characteristics of membrane and micelle-bound proteins.

This study concerns calbindin D_{9k} (S100D), a small EF-hand Ca^{2+}-binding protein from the S100 subfamily, that binds two Ca^{2+} with micromolar affinity and high cooperativity. It is found in epithelial cells of the small intestine and placenta, where it is believed to take part in uptake and transcellular transport of Ca^{2+} (*2*−*5*), and in mineral nucleation in matrix vesicles of epiphyseal cartilage and bone (*6*). An interaction of calbindin D_{9k} with lyso-phosphatidylcholine (lyso-PC),[1] which is abundant in the intestinal brush-border membrane has been reported (*7*). Although the transport mechanism of Ca^{2+} bound by calbindin D_{9k} is not known, it is conceivable that it is modulated by direct interactions with phospholipid monomers and aggregates, including the cell membrane.

Calbindin D_{9k} consists of two helix−loop−helix EF-hand motifs connected by a linker segment and a β-type interaction between the Ca^{2+}-binding sites (Figures 1A and 1B). The C-terminal Ca^{2+}-binding loop conforms to the regular 12-residue EF-hand Ca^{2+}-binding loop (II) that uses mainly side-chain oxygen atoms for coordination (*8*, *9*). The N-terminal loop (I) on the other hand has the so-called *pseudo* EF-hand sequence unique to the N-terminal EF-hands of the S100 proteins, with a 14-residue Ca^{2+}-binding loop that uses primarily main-chain oxygen atoms for ion coordination (*10*, *11*). Its structure, dynamics, and other biophysical properties have been examined in great detail (e.g., *12*−*23*).

Recent *in vitro* studies of proteins using detergents such as dodecyl phosphocholine (DPC) or sodium dodecyl sulfate (SDS) have revealed that interactions of detergents with water-soluble helical proteins may involve two phases. The detergent is found to interact locally with a specific set of hydrophobic residues in some proteins at low detergent concentrations and then transforms the protein to a "molten-globule-like" micelle bound form above the critical micelle concentration (cmc) (e.g., *24*, *25*).

To obtain insights into the interaction of calbindin D_{9k} with phospholipid monomer, micelle, or membrane substrates and to further probe the biophysical properties of the protein,

† This work was supported by an operating grant from the National Institutes of Health (GM40120), the Vanderbilt Center in Molecular Toxicology (NIH P30 ES00267), the Danish Natural Science Research Foundation (SNF), and the Danish Biotechnological Instrument Centre (DABIC), and fellowships to A.M. from the Swedish Foundation for International Cooperation in Research and Higher Education (STINT) and from Carlsbergfondet.

* To whom correspondence should be addressed. Telephone: +45-8942-3866. Fax: +45-8619-6199. E-mail: anders@chem.au.dk (A.M.); Telephone: 615-936-2209. Fax: 615-936-2211. E-mail: walter.chazin@vanderbilt.edu (W.J.C.).

‡ Vanderbilt University.

§ University of Aarhus.

[1] Abbreviations: CHAPS, 3-[(3-cholamidopropyl-dimethylammonio)]-1-propane-sulfonate; cmc, critical micelle concentration; DNS, 1-(dimethylamino)naphthalene-5-sulphonate; DPC, dodecyl phosphocholine; lyso-PC, lyso-phosphatidylcholine; SDS, sodium dodecyl sulfate.

10.1021/bi050088z CCC: $30.25 © 2005 American Chemical Society
Published on Web 04/09/2005

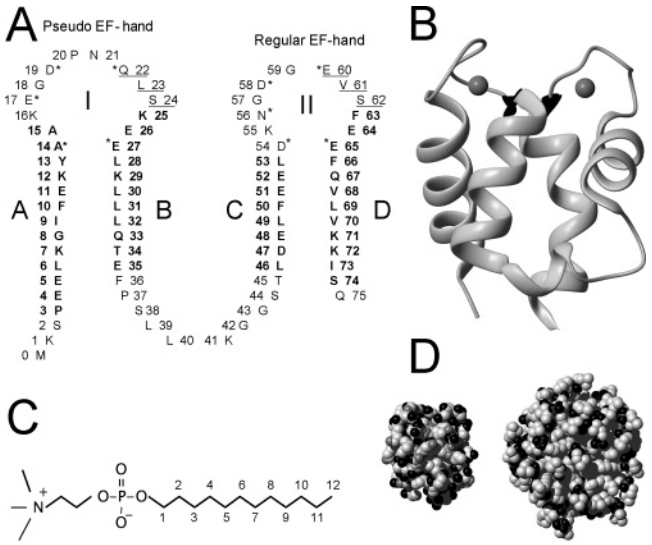

FIGURE 1: Amino acid sequence and structures of P43G calbindin D_{9k} and DPC micelles. (A) $(Ca^{2+})_2$ calbindin D_{9k} secondary structure (*23*) is indicated with **α-helical** residues in boldface and β-sheet residues underlined. Residues coordinating Ca^{2+} are marked with an asterisk. (B) Ribbon diagram of Ca^{2+}-loaded calbindin D_{9k} (*70*). (C) Chemical structure of dodecyl phosphocholine (DPC). (D) Space filling models of calbindin D_{9k} (left) and an MD-simulated structure of a DPC micelle consisting of 54 monomers (*71*) (right). Oxygen, phosphorus, nitrogen, and carbon atoms are colored black, dark gray, gray, and light gray, respectively. The molecular graphics in this paper were prepared using MOLMOL (*72*).

we have used NMR to explore the interaction between calbindin D_{9k} and DPC below and above the cmc, the influence of pH, and the presence of Ca^{2+} (Figure 2).

MATERIALS AND METHODS

Sample Preparation. Uniformly ^{15}N-labeled P43G[2] calbindin D_{9k} was expressed in *Escherichia coli* and purified as reported previously (*26*, *27*). DPC was purchased from Avanti (Avanti Polar Lipids, Alabaster, AL).

NMR Spectroscopy. The NMR experiments were conducted at 300 K using Bruker Avance spectrometers operating at proton frequencies of 500.13 and 600.21 MHz. Titrations of calbindin D_{9k} with DPC in the absence and presence of Ca^{2+} were followed by 2D ^{15}N-^1H HSQC spectroscopy (*28*). All samples contained 0.04−0.15 mM calbindin D_{9k}, 20 mM KCl, 20 mM Tris, and 100 μM NaN_3. DPC and pH titrations were made on apo (1 mM EDTA; 0−40 mM DPC at pH 7.4; pH 7.4−4.0 at 40 mM DPC) and Ca^{2+}-loaded calbindin D_{9k} samples (4 mM $CaCl_2$; 0−40 mM DPC at pH 7.4 and 4.0; pH 7.4−1.7 at 40 mM DPC). DPC was added in aliquots of 0.05, 0.2, and 1 M DPC in 20 mM KCl, 20 mM Tris, and 100 μM NaN_3, and pH was adjusted with aliquots of 1 M HCl and NaOH, respectively. The DPC solutions were prepared by mixing dry DPC powder with buffer. Exchange spectroscopy was carried out in the presence of Ca^{2+} at 10 mM DPC at pH 4.7 using a 2D HSQC experiment with a ZZ-exchange delay of 200 ms inserted between the evolution and acquisition periods (1024 scans, 2048 × 256 complex points) (*29*, *30*). 3D TOCSY−HSQC (68 ms) and 3D NOESY−HSQC (100 ms) experiments (*31*, *32*) (16 scans, 1024 × 16 × 80 complex points) of apo calbindin D_{9k} in 40 mM DPC at pH 4.0 were collected. ^1H chemical shifts were referenced to the ^1H_2O resonance at 4.736 ppm at 300 K (*33*, *34*), and ^{15}N chemical shifts were referenced indirectly via the ^1H frequency using the frequency ratio ($^{15}N/^1H$) of 0.101 329 118 (*35*).

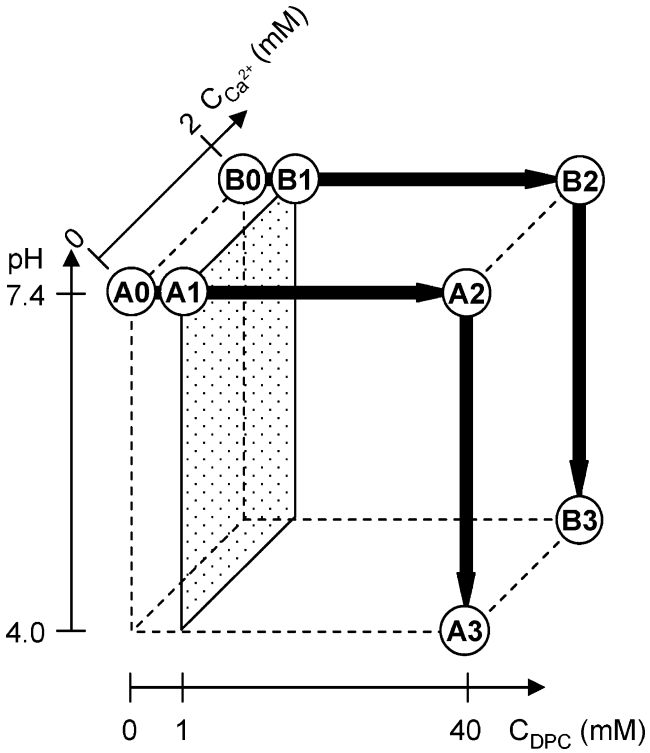

FIGURE 2: Schematic overview of the titration experiments monitored by NMR and CD. Titration of apo calbindin D_{9k} with increasing amounts of DPC (A0−A2) and subsequent lowering of pH (A2−A3). Titration of Ca^{2+}-loaded calbindin D_{9k} with increasing amounts of DPC (B0−B2) and subsequent lowering of pH (B2−B3). The shadowed plane marks the cmc.

NMR Data Processing and Analysis. NMR data were processed using *NMRPipe* (*36*), with pure cosine window functions and zero-filling to double size in both dimensions. Assignments of H^N and N^H resonances at the various stages of the titration were made using *NMRVIEW* (*37*).

Hydrophobic Moment Calculations. The average per residue hydrophobic moment $\bar{\mu}_H$ for ideal α helices was calculated as (*38*, *39*)

$$\bar{\mu}_H = \frac{1}{N}\sum_i^N H_i \mathbf{r}_i \qquad (1)$$

where H_i is the transfer free energy of the ith residue in an α helix from the membrane interior to water (*40*) and $\mathbf{r}_i$ is the normalized vector through the C^α and perpendicular to the helical axis.

CD Experiments. CD measurements were conducted in 10 mm quartz cuvettes using a Jasco J-720 spectropolarimeter (Jasco Inc., Easton, MD). CD spectra were recorded as a function of added DPC in the absence of Ca^{2+} at pH 7.4 and in the presence of Ca^{2+} at pH 4.0 and 7.4. Spectra were collected in three scans from 170 to 300 nm with a step size of 1 nm, an average time of 2 s for each point, and background correction against a buffer blank.

[2] To avoid cis−trans isomerism around the P43−S44 bond, the P43G mutant was used (*1*).

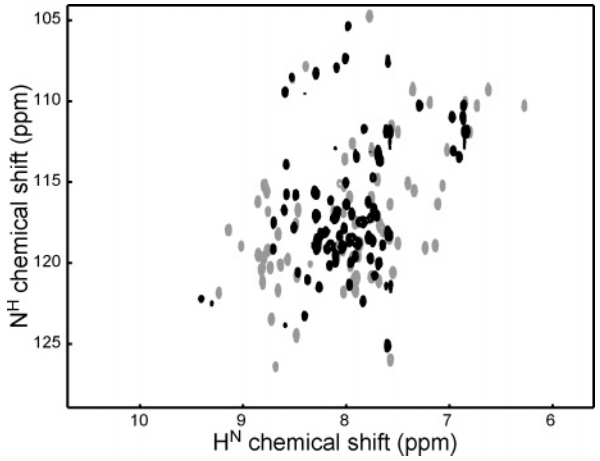

FIGURE 3: Spectral changes in apo calbindin D_{9k} are induced by association with DPC micelles. ^{15}N-^{1}H HSQC spectra of apo calbindin D_{9k} in the absence (gray; pH 7.4) and presence (black; pH 4.0; 40 mM) of DPC micelles (cf. Figure 2, A0 and A3).

RESULTS

Overview of the DPC Titrations. The impact of increasing concentrations of DPC on calbindin D_{9k} in the absence and presence of Ca^{2+} and at different pH is manifested in changes in the appearance of ^{15}N-^{1}H HSQC spectra.

Addition of DPC in the Absence of Ca^{2+}. When DPC is added to apo calbindin D_{9k} at neutral pH (7.4), only very subtle spectral changes occur below the cmc (cf. Figure 2, A0−A1). There is thus no sign of interactions with individual DPC molecules. However, when DPC micelles start forming as the DPC concentration is raised above the cmc (1 mM), an interaction manifests itself by significant broadening of most protein signals, some of which disappear (cf. Figure 2, A1). At a DPC concentration of 10 mM, roughly corresponding to 70 DPC molecules per protein molecule, most signals have reappeared at a new position, indicating that a significant population of the protein has shifted to a new micelle-associated state. Many of the signals are broad and remain broad also at a 4 times higher DPC concentration (corresponding to almost 300 DPC molecules per protein molecule; cf. Figure 2, A2). However, if the pH is decreased (Figure 2, A2−A3), the signals sharpen up with significant changes already apparent at pH 7. This behavior may either be caused by changes in the equilibrium populations and/or exchange rates between different micelle-associated states or between micelle-associated and micelle-free states (*vide infra*). Figure 3 shows spectra of apo and micelle-associated calbindin D_{9k}.

Addition of DPC in the Presence of Ca^{2+}. The scenario is quite different when DPC is added to a solution of Ca^{2+}-saturated protein at neutral pH (7.4). Here, the specific binding of individual DPC molecules results in changes in the chemical shifts of a specific set of mainly hydrophobic residues in the protein core below the cmc (Figure 4, cf. Figure 2, B0−B1). The apparent midpoint is 0.9 mM DPC, and the process saturates at ∼10 mM DPC (Figure 5). Unlike the apo state, no other changes are observed: there is no trace of an interaction between the protein and the DPC micelles even at 40 mM DPC (cf. Figure 2, B2). However, if the pH of the Ca^{2+}- and DPC-saturated sample is lowered (Figure 2, B2−B3), micelle binding can better compete with Ca^{2+} binding and a transition to a micelle-associated state occurs with a midpoint around pH 5. At this pH, binding of Ca^{2+} to site II causes the signals corresponding to the residues around this site in the micelle-associated state to disappear or significantly broaden. When the pH is lowered further, Ca^{2+} leaves the site and the broadened signals appear and sharpen. Around pH 4, the spectrum is virtually identical to that obtained at similar pH in the absence of Ca^{2+} and it is assumed that no Ca^{2+} is bound to the protein (cf. Figure 2, B3 and A3; data not shown). No further spectral changes occur when the pH is lowered to 1.7.

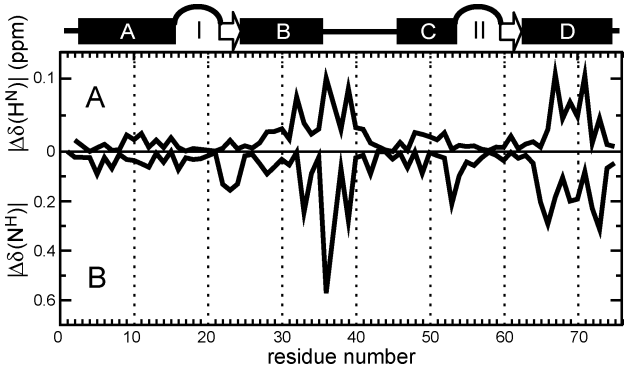

FIGURE 4: Binding of individual DPC molecules to Ca^{2+}-loaded calbindin D_{9k}. Absolute changes in (A) H^N and (B) N^H chemical shifts when DPC molecules bind to Ca^{2+}-loaded calbindin D_{9k}. The α helices are represented by dark rectangles; the *β* strands, by open arrows; and the Ca^{2+}-binding loops, by arcs.

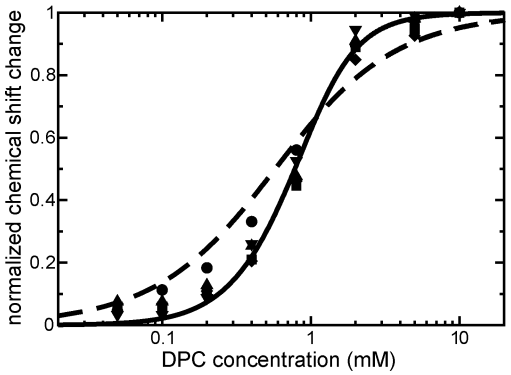

FIGURE 5: Normalized DPC molecule-binding curves for residues in $(Ca^{2+})_2$ calbindin D_{9k}. Data are shown for $F36N^H$ (●), $Q67H^N$ (■), $Q67H^{\epsilon 21}$ (◆), $K71H^N$ (▲), and $I73N^H$ (▼). Theoretical curves for one site binding with a K_D of 0.5 mM (- - -) and two site binding with infinite cooperativity and a mean K_d of 0.63 mM (—) are shown for comparison.

At various points during these experiments, CD spectroscopy was used to establish that the overall helical content in the protein was not significantly perturbed (data not shown).

Chemical-Shift Assignments: Ca^{2+}-Loaded Calbindin D_{9k} Interacting with Individual DPC Molecules. The association of individual DPC molecules to Ca^{2+}-loaded calbindin D_{9k} is fast on the NMR chemical-shift time scale (*vide infra*), and all resonances of the state with a DPC-molecule bound could be assigned using the chemical-shift assignment of the Ca^{2+}-loaded state (*41*, *42*) by following the signals as they move as a function of added DPC.

Micelle-Associated Apo Calbindin D_{9k}. In the transition from the apo to the micelle-associated state, many of the resonances undergo slow-to-intermediate exchange and cannot be followed from one state to the other (*vide infra*). Consequently, chemical-shift assignment for the micelle-

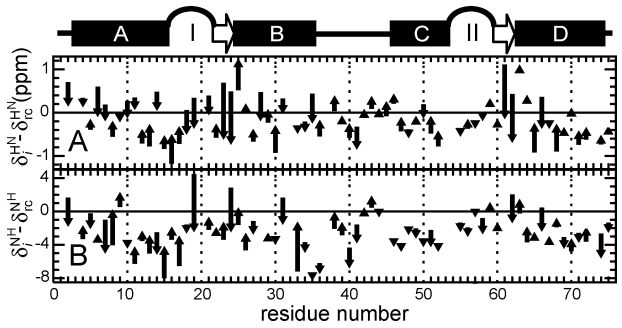

FIGURE 6: Backbone amide chemical-shift changes in apo calbindin D_{9k} induced by association with DPC micelles. The changes in (A) H^N and (B) N^H chemical shifts are shown relative to calculated random-coil values. The chemical-shift changes occurring upon micelle association are indicated with arrows, starting at the apo-state shifts and ending at the shifts of the micelle-associated state. The random-coil shifts were calculated using the SIMPRED web server at redpoll.pharmacy.ualberta.ca (*44*).

associated state had to be obtained. A majority, 77 of 86 (65 of 74 backbone and all 12 side chain) ^{15}N-^{1}H correlations and 71 of 76 H^α could be assigned. Many resonances were assigned using the chemical-shift assignment of the apo state (*42*, *43*) by following the signals as they move as a function of added DPC. Others were assigned by exchange experiments (*vide infra*). The assignments were verified, and most of those not yet assigned were assigned using the 3D TOCSY−HSQC and 3D NOESY−HSQC spectra of calbindin D_{9k} acquired in 40 mM DPC at pH 4.0 in the absence of Ca^{2+} (cf. Figure 2, A3).

Analysis of Chemical-Shift Perturbations. To provide information about how calbindin D_{9k} interacts with individual DPC molecules as well as with DPC micelles, we have analyzed the chemical-shift changes for the amide protons (H^N) and nitrogens (N^H) induced by these interactions.

Interactions between Ca^{2+}-Loaded Calbindin D_{9k} and Individual DPC Molecules. The chemical-shift changes that occur upon DPC association in the presence of Ca^{2+} are relatively moderate (Figure 4, cf. Figure 2, B0−B2). The largest chemical-shift changes [$0.07 < \delta(H^N) < 0.1$ or $0.28 < \delta(N^H) < 0.6$ ppm] occur for L32, F36, L39, F66, Q67, K71, and I73 (Figure 4). These residues map to a hydrophobic cluster around the linker, pointing to a specific binding site (*vide infra*).

Interactions between Apo Calbindin D_{9k} and DPC Micelles. The chemical-shift changes that occur upon DPC−micelle association of apo calbindin D_{9k} are much more significant than those for binding of individual DPC molecules to the Ca^{2+}-loaded state (Figures 3 and 6, cf. Figure 2, A0−A2) and include a significant reduction in the chemical-shift dispersion.

The chemical-shift changes between free and micelle-associated calbindin D_{9k} are as large as 1.2 and 5.3 ppm for H^N and N^H, respectively (Figure 6). The largest chemical-shift changes [$|\Delta\delta(H^N)| > 1$ ppm or $|\Delta\delta(N^H)| > 4$ ppm] are measured for D19, L23, S24, and Q33 in EF-hand I and for V61 and S62 in EF-hand II. Four of these (L23, S24, V61, and S62) participate in the β-type interaction between the Ca^{2+}-binding loops. Outside of the β-type interactions, the most important H^N chemical-shift changes occur in helix A, B, and D and loop I, while helix C and loop II are largely unaffected. For N^H, the largest changes occur in helix A and loop I. The average changes in chemical shift for the individual secondary structure elements are shown in Table 1.

Table 1: Average Chemical-Shift Changes upon Interaction of Apo Calbindin D_{9k} with DPC Micelles[a], Calculated Using Absolute Values for H^N, N^H, and H^α and with a Sign for H^α

structural element[b]	$\lvert\Delta\delta(H^N)\rvert$ (ppm)	$\lvert\Delta\delta(N^H)\rvert$ (ppm)	$\lvert\Delta\delta(H^\alpha)\rvert$ (ppm)	$\Delta\delta(H^\alpha)$ (ppm)
all	0.27 ± 0.03	1.23 ± 0.16	0.17 ± 0.03	0.02 ± 0.03
helix A	0.23 ± 0.04	1.61 ± 0.34	0.17 ± 0.05	0.04 ± 0.03
helix B	0.30 ± 0.07	1.41 ± 0.55	0.21 ± 0.12	0.09 ± 0.07
helix C	0.16 ± 0.03	0.37 ± 0.18	0.04 ± 0.01	0.15 ± 0.13
helix D	0.21 ± 0.07	0.97 ± 0.22	0.22 ± 0.08	0.01 ± 0.02
β sheet	0.78 ± 0.21	1.82 ± 0.87	0.47 ± 0.14	0.21 ± 0.08
loop I	0.43 ± 0.06	2.27 ± 1.09	0.24 ± 0.08	-0.45 ± 0.15
loop II	0.04 ± 0.02	0.47 ± 0.20	0.04 ± 0.01	-0.04 ± 0.14
linker	0.17 ± 0.04	0.90 ± 0.22	0.08 ± 0.02	-0.02 ± 0.02

[a] The limits are standard deviations of the mean. [b] Helices: A, 3−15; B, 25−35; C, 46−53; and D, 63−74. β sheet: 22−24 and 60−62. Loops: I, 16−21; and II, 54−59. Linker: 36−45.

Figure 6 shows an analysis of changes in NMR chemical shifts of apo calbindin D_{9k} upon association with a micelle. The H^N and N^H chemical shift are normalized to the random-coil values calculated using the SIMPRED web server at redpoll.pharmacy.ualberta.ca (*44*). The data show that the apo protein deviations from random-coil chemical shifts have a far larger spread than the micelle-associated protein, suggesting a lower level of tertiary interactions for the latter.

H^α and side-chain proton chemical shifts typically exhibit a smaller degree of scatter than H^N chemical shifts because of their lower sensitivity to differences in local parameters such as pH and ionic strength. On the other hand, H^α chemical shifts have a well-explored relation to the backbone conformation of the protein (*45*). L31 displays the largest H^α chemical-shift (+1.2 ppm) difference upon association with a micelle. This residue has a uniquely low chemical shift in the absence of DPC (2.3 and 2.9 ppm with and without Ca^{2+}, respectively) because of ring-current effects from the closely packed aromatic ring of Y13. The return of this chemical shift back to a value much closer to the random coil is consistent with a loss of tertiary structure upon association with micelles. Residues N21, Q22, L23, E60, and S62, which are part of the cross-strand β-type interaction in the native folded protein (Figure 1) also show important changes toward random-coil values, indicating the loss of the β interaction. The average H^α chemical shifts of all non-β-strand residues are 4.11 ± 0.05 and 4.14 ± 0.04 ppm, in the apo and micelle-associated states, respectively, which shows that the helical secondary structure is not significantly different, consistent with the results from CD spectroscopy.

When comparing the H^α chemical shifts of micelle-associated and apo calbindin D_{9k} with the random-coil values (*44*), the profiles shown in Figure 8 are obtained. The patterns are very similar except that all residues in the β strands do not display the chemical shifts typical of a β interaction in the micelle-associated state, except for S62. The helices are essentially unaltered, with small changes in length (e.g., helix A appears to stop already at A14). Many of the residues in helix A and D show higher H^α chemical shifts in the micelle-associated state, although they are still in the α-helical range. Many residues in loop I are affected, whereas almost no changes are observed between L40 in the middle of the linker

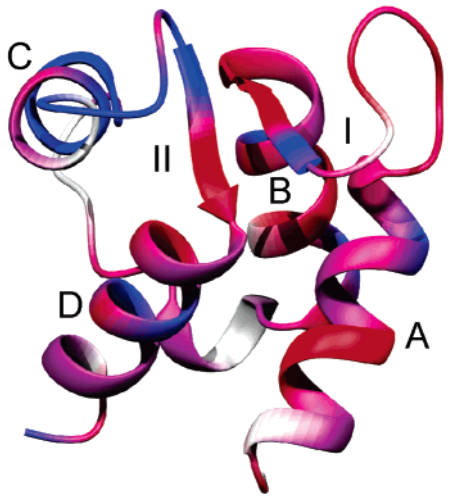

FIGURE 7: Structural mapping of H^N and N^H chemical-shift changes in calbindin D_{9k} (*70*) upon association with DPC micelles. Residues are colored from red to blue according to the highest magnitude of the experienced H^N and N^H chemical-shift change (after dividing the N^H changes by 4). Red indicates a large change [$\Delta\delta(H^N) > 0.8$ and $\Delta\delta(N^H) > 3.6$ ppm], and blue indicates a small change [$\Delta\delta(H^N) < 0.2$ and $\Delta\delta(N^H) < 0.8$ ppm], while gray indicates that the chemical-shift change was not determined.

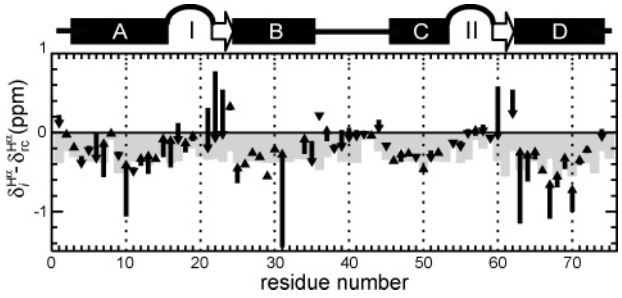

FIGURE 8: H^α chemical-shift changes in apo calbindin D_{9k} induced by association with DPC micelles. The chemical shifts are normalized relative to the calculated random-coil values. The chemical-shift changes occurring upon micelle association are indicated with arrows, starting at the apo-state shifts and ending at the shifts of the micelle-associated state. Calculated chemical shifts for α helices are indicated with gray bars. The random coil and α-helical chemical shifts were calculated using the SIMPRED web server at redpoll.pharmacy.ualberta.ca (*44*).

and second β strand (i.e., the C-terminal half of the linker, helix C, and most of loop II).

NOE Contacts. Because of a combination of severe overlap and relatively low resolution in the indirect dimension of the NOESY−HSQC spectrum, few sequential NOE contacts could be unambiguously assigned. A total of 47 $H^N_{(i)}-H^N_{(i+1)}$, 36 $H^\alpha_{(i)}-H^N_{(i+1)}$, 12 $H^\alpha_{(i)}-H^N_{(i+2)}$, 6 $H^\alpha_{(i)}-H^N_{(i+3)}$, and no $H^\alpha_{(i)}-H^N_{(i+4)}$ were identified. Many of the $i-i+2$ contacts were located in loop I and the linker region, while the $i-i+3$ contacts were scattered through the protein except for three contacts between E65−V68 and V68−K71 in the middle of helix D (data not shown).

Many of the H^N resonances show NOEs to water and to the strong signal from the aliphatic protons on carbon 3−10 of DPC (H^{3-10}) (Figures 1C and 9). The strongest water NOEs appear at the termini and at the beginning of helix B. Helices C and D show water NOEs with a periodicity that might suggest a location on the micelle surface. Helix A and loop I and II show almost no contacts with water, suggesting that they are buried deeper down in the micelle. Most of the

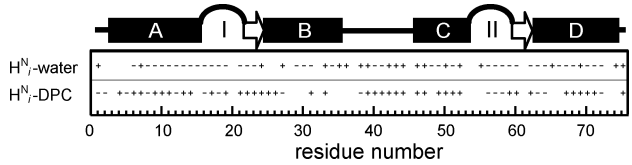

FIGURE 9: NOEs between H^N and water and DPC protons. Symbols: +, present; −, absent.

H^N resonances, with the exception of the N-terminal part of loop II, show NOEs to the H^{3-10} of DPC. Here, the NOEs for helix A show a periodicity that might suggest a location on the micelle surface.

Equilibria and Exchange Rates. During the NMR experiments, the protein is undergoing a number of chemical-exchange processes between different states, some of which involve interactions with Ca^{2+}, individual DPC molecules, and DPC micelles. Many of these processes occur with an exchange rate that is comparable to the NMR chemical-shift difference between the exchanging states. For exchange between two states,

$$k_{ex} \approx \Delta\omega = \gamma B_0 \Delta\delta \qquad (2)$$

where k_{ex} ($=k_1 + k_{-1}$) is the exchange rate between the two states; $\Delta\omega$, the angular frequency difference between the resonances corresponding to the two isolated states; γ, the gyromagnetic ratio; B_0, the external magnetic field; and $\Delta\delta$, the chemical-shift difference between the two states. Exchange processes on this time scale influence the positions and line widths of the resonance, and dynamic information can be extracted from these.

When the rate of exchange is slow, two discrete peaks appear at the positions corresponding to the NMR chemical shifts of the two states. The broadening of resonances is $k_{ex}(1-p)$, where p is the relative population of that state. When the rate of exchange is fast, one signal appears at a position that is the population-weighted average of the two states and with line broadening of $p(1-p)(\Delta\omega)^2/k_{ex}$. Between these two regimes, the full Bloch−McConnel equations (*46*) can be used to evaluate the data (*47*).

Interactions between Ca^{2+}-Loaded Calbindin D_{9k} and Individual DPC Molecules. When single DPC molecules associate with Ca^{2+}-loaded calbindin D_{9k} at neutral pH (7.4) (Figure 2, B0−B2), the exchange process occurs with a rate that is fast compared to $\Delta\omega$. Thus, only one set of signals is observed with no excess line broadening. Because no detectable line broadening is observed for $Q67H^{\epsilon 21}$, which undergoes the largest chemical-shift change (80 Hz), the off-rate of DPC from Ca^{2+}-loaded calbindin D_{9k} must be faster than 10^5 s^{-1}.

The measured chemical shifts are the population-weighted mean values of the chemical shifts of the free and associated states. Thus, the relative populations can be estimated from the normalized chemical-shift changes [i.e., $(\delta-\delta_0)/(\delta_\infty-\delta_0)$, where δ, δ_0, and δ_∞ are the chemical shifts at a particular titration point and at the start and end of the titration, respectively] determined by following the binding curve to saturation. Using this approach, Ca^{2+}-loaded calbindin D_{9k} appears to bind more than one DPC molecule cooperatively: the slope of the binding curve in Figure 5 exceeds that possible for binding of a single molecule. A mean dissociation constant (K_d) of 0.5 mM is derived from Figure

5. Above the cmc (~1 mM), DPC−micelle formation competes with DPC molecule association, so the later part of the binding curve is probably shallower than it would be in the absence of micelle formation. It is also conceivable that the saturation point of the curve in Figure 5 does not represent a fully saturated binding site. However, regardless of the details of the later stages of the binding curve, the shape of the curve below cmc clearly shows that more than one DPC molecule is involved. Data collected at pH 4 indicate that the interaction between calbindin D_{9k} and DPC is the same at acidic pH.

Interactions between Apo Calbindin D_{9k} and DPC Micelles. When apo calbindin D_{9k} interacts with DPC micelles at pH 7.4 (Figure 2, A1−A2), the protein exhibits intermediate exchange between the free and DPC micelle-associated states. The exchange rates are similar to $\Delta\omega$, i.e., on the order of 1000 s^{-1}. However, the individual signals do not move linearly with an increasing DPC concentration, indicative of contributions from more than two states. Therefore, more than one micelle state must be considered. The excess line broadening observed in the range 10−40 mM DPC is caused by residual exchange processes occurring throughout this range. Sharper signals at lower pH can be attributed to a shift in the equilibrium toward one dominating state or to a faster exchange between the different states.

Interactions between Ca^{2+}-Loaded Calbindin D_{9k} and DPC Micelles. When the pH of Ca^{2+}-saturated calbindin D_{9k} in the presence of a large excess of DPC micelles is decreased from neutral (Figure 2, B2−B3), a transition to a micelle-associated state occurs and gives rise to a second set of peaks. Under the conditions used here, the transition has a midpoint around pH 5 and occurs at a time scale that allows recording of exchange cross-peaks (*29*, *30*) (Figure 10A). The exchange cross-peaks (200 ms exchange delay) provide partial assignment of the membrane-associated state. Interestingly, these are all located in EF-hand I and the linker with the exception of the C-terminal residues K71−Q75 (Figure 10B). The time scale of the exchange process can be evaluated from the relative intensities of the exchange and autocorrelation cross-peaks

$$\frac{I_{CaDPC}}{I_{CaCa}} = \frac{p_{DPC}\{1 - \exp(-k_{ex}\tau)\}}{p_{Ca} + p_{DPC}\exp(-k_{ex}\tau)} \qquad (3)$$

where I_{CaCa} is the intensity of the N−H autocorrelation cross-peak for the calcium-loaded DPC-free state, I_{CaDPC} is the intensity of the N−H exchange cross-peaks between the calcium-loaded DPC-free state and the DPC-associated state, p_{Ca} and p_{DPC} are the populations of the two states, and τ is the exchange delay (*47*). At pH 5, a population of about 60% in the DPC−micelle-associated state is estimated from peak intensities in the HSQC spectrum. The exchange peaks in the 200 ms exchange spectrum show exchange peaks of approximately 40% of the intensity of the peaks corresponding to the DPC−micelle-associated state. An exchange rate k_{ex} of 6 ± 3 s^{-1} can be estimated using eq 3.

The absence of exchange peaks for some of the residues that show two sets of peaks at pH 5 suggests that they exchange too slowly to be characterized in the exchange experiment. This would imply an exchange rate of less than about 0.5 s^{-1} (for <5% intensity). However, many of the residues in and around loop II, where relatively large chemical-shift changes are measured or expected, do not yield detectable signals for the micelle-associated state at this pH with Ca^{2+} present but appear when pH is further decreased. The site thus appears to be subject to a more complicated exchange process than the slow *pseudo* two-state process experienced by the residues in EF-hand I. The location around EF-hand site II suggests that the exchange process is related to residual Ca^{2+} association at this site.

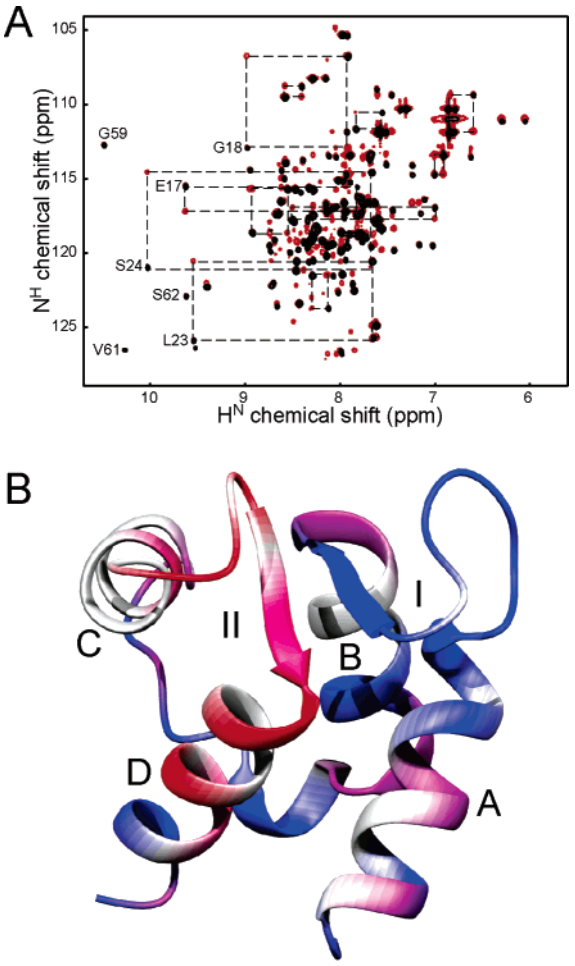

FIGURE 10: Exchange between $(Ca^{2+})_2$-loaded and micelle-associated calbindin D_{9k}. (A) HSQC (black) and exchange HSQC (red) spectra at pH 5 in the presence of Ca^{2+} and DPC micelles (cf. Figure 2, B2−B3). Some of the protons that are most downfield-shifted in the Ca^{2+}-loaded state are labeled with the residue name, and some of the residues showing exchange peaks are labeled with boxes. Note that the downfield-shifted residues in loop I show exchange peaks, while those in loop II do not. (B) Structural mapping of the exchange behavior at pH 5 in the presence of Ca^{2+} and DPC micelles. Blue represents residues with exchange peaks corresponding to an exchange rate of ~6 s^{-1} between Ca^{2+}-loaded and micelle-associated calbindin D_{9k}; violet, residues for which no exchange peaks were identified; pink, residues for which there are clearly no exchange peaks; and red, residues for which signals corresponding to the micelle-bound state are broadened beyond detection.

DISCUSSION

Interaction with Isolated DPC Molecules. Isolated DPC molecules associate with a hydrophobic cluster in Ca^{2+}-loaded calbindin D_{9k}. The interaction involves two or more DPC molecules. At neutral pH (7.4), the dissociation constant (K_d) is 0.5 mM or weaker and the off rate is faster than ~10^5 s^{-1}. The induced chemical-shift differences at the apparent

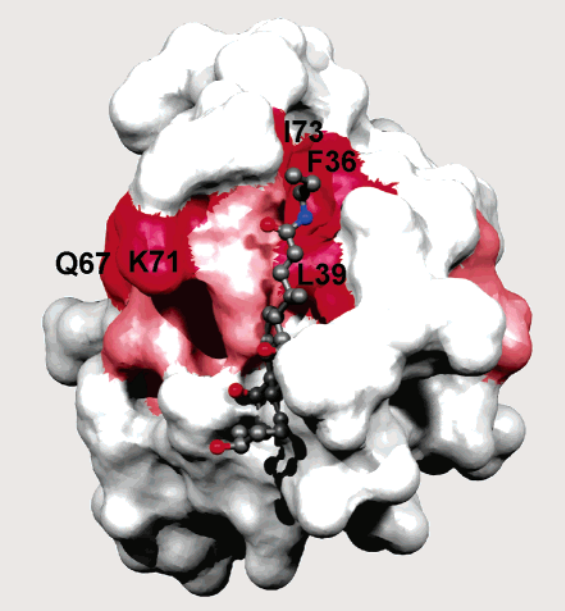

FIGURE 11: Structural mapping of the site of interaction with individual DPC molecules in Ca^{2+}-loaded calbindin D_{9k}. Residues experiencing the largest chemical-shift changes are shown in red [$\Delta\delta(H^N) > 0.06$ and $\Delta\delta(N^H) > 0.24$ ppm], and smaller changes [$0.06 > \Delta\delta(H^N) > 0.04$ and $0.24 > \Delta\delta(N^H) > 0.16$ ppm] are shown in pink. Three of the hydrophobic residues with the highest chemical-shift changes (F36, L39, and I73) form a cluster at the surface. The other two (L32 and F66) are not surface-exposed. A CHAPS molecule from the structure of S100A9 (*48*) was modeled onto the structure of calbindin D_{9k} (*70*) by aligning helices B, C, and D of the two proteins.

saturation point are small, indicating that DPC molecules bind without any significant alteration of the structure. The fact that only binding to the Ca^{2+}-loaded state is detected suggests that a hydrophobic "patch" suitable for DPC binding is formed upon Ca^{2+} binding. The involvement of more than one DPC molecule may reflect that one molecule is not sufficiently large to saturate this "patch".

The Ca^{2+} dependence agrees well with significant Ca^{2+}-induced reorganization of the packing of some of the residues involved (*22*). Furthermore, the Ca^{2+}-dependent formation of a small hydrophobic patch on calbindin D_{9k} provides an explanation for the 25-fold increase in Ca^{2+} affinity when one of the phenylalanines involved in the DPC interaction, F66, is changed to a tryptophan (*17*). The larger tryptophan side chain presumably stabilizes the Ca^{2+}-loaded state by filling part of the proposed Ca^{2+}-induced hydrophobic surface, thus increasing the Ca^{2+} affinity relative to the wild-type protein.

Interestingly, a recent X-ray structure of the Ca^{2+}-loaded homodimeric form of the protein S100A9 (MRP14) shows a molecule of the detergent CHAPS bound to a hydrophobic patch at a similar position in the linker (*48*). Two of the residues experiencing the largest chemical-shift changes in the present study (L39 and I73) are homologous to residues in direct contact with the CHAPS molecule. As shown in Figure 11, where a CHAPS molecule from the S100 A9 structure (*48*) has been positioned relative to the calbindin D_{9k} structure by overlaying helices B, C, and D of the two proteins, the interaction surface suggested by the changes in chemical shifts does not cover the entire surface that would be exposed to CHAPS. L49 and other residues in helix C that cover this surface at the lower end in Figure 11 show smaller chemical-shift changes. The interaction with DPC is thus limited to the cleft between helix B and D, but because a DPC molecule is about half the size of CHAPS (351 relative to 615 Da), the surface should be large enough to interact with DPC molecules.

Interaction with DPC Micelles: Determinants of Micelle Association. Calbindin D_{9k} associates with DPC micelles in the absence of Ca^{2+}. The evidence of protein−micelle complex formation is overwhelming: the transition only occurs above the cmc for DPC; a new equilibrium state is reached when there in theory should be a little bit more micelles than proteins; NOE contacts to DPC occur throughout the complexed protein; and the NMR spectrum changes in the same way as in previous studies of micelle-association.

The interaction is pH-dependent: the structural heterogeneity at neutral pH, illustrated by the many broad resonances seems to disappear when pH is decreased. Although the narrower signals could also be explained by a faster exchange between similarly populated states, it is more likely that there actually is a stabilization of one state, because of the reduction in charge and folding stability at lower pH (*vide infra*). An additional factor leading to increasing homogeneity among the micelle-associated states might be the lower number of charges that simultaneously need to find a suitable polar environment.

DPC micelle association can also better compete with Ca^{2+} binding at lower pH (cf. Figure 2, B2−B3). This is in part because the Ca^{2+} affinity decreases at acidic conditions (*49*). At pH 5 (0.04 mM protein, 1 mM Ca^{2+}, and 10 mM DPC), we can measure roughly equal populations of the micelle-associated and Ca^{2+}-bound states. We can estimate an apparent average Ca^{2+} dissociation constant for the two Ca^{2+} sites of around 1 mM. The values of the Ca^{2+} dissociation constants are highly dependent on solution conditions such as pH (*49*) and ionic strength (*19*). For example, Ca^{2+} binding will be affected by electrostatic screening from charges on the micelles. On the basis of previously reported data (*19*, *49*), the Ca^{2+} dissociation constants can be estimated to be of the order of 5 μM at these conditions.

The aggregation number of DPC micelles is approximately 56 (*50*), resulting in 19-kD micelles (Figure 1D), although the aggregation number of a protein−micelle system may deviate significantly from that of the protein-free micelle (*51*). With the concentrations in the titration made in the absence of Ca^{2+}, there are about 7 DPC molecules per protein molecule at the cmc (1 mM), roughly corresponding to 1 micelle per 8 protein molecules. Hypothetically, a ratio of 1 micelle per protein molecule is obtained at 8.25 mM DPC. This explains why most of the protein resonances are exchanging between different states at DPC levels just above cmc and agrees well with the saturation of many signals at 10 mM DPC in the absence of Ca^{2+}.

To estimate the strength of the micelle−protein interaction, an approximate "micelle−protein dissociation constant" can be determined at conditions (pH 5, 0.04 mM protein, 1 mM Ca^{2+}, and 10 mM DPC) where the population of both the micelle-associated and Ca^{2+}-bound states (60 and 40%, respectively) can be measured. Two assumptions are made: (i) each micelle contains 56 DPC molecules, which corresponds to 0.18 mM micelle in the sample, and (ii) only one of the two Ca^{2+} ions needs to be released from the protein

to allow micelle association. Under these conditions, the dissociation constant for the micelle−protein complex is 0.16 times that of the dissociation constant of the first Ca^{2+} ion. A Ca^{2+} dissociation constant on the order of 5 μM (*vide supra*) yields a micelle−protein dissociation constant around 0.8 μM. It is important to note that, in fact, the micelle−protein affinity is expected to be stronger than this value because it is likely that the second Ca^{2+} ion also needs to be released from the protein to reach full micelle affinity.

One central question is how general the behavior described here is, and what the determinants for association with a micelle, vesicle, or membrane are. Micelle, vesicle, or liposome association as a one-step cooperative process has been documented for a number of proteins including: cytochrome *c*, bovine serum albumin, and lysozyme (*52*, *53*). There are many examples in the literature of proteins that associate with micelles at acidic pH. The reason for the pH dependence was addressed by de Alba et al. (*54*) in a study of the lysosomal protein saponin C, which activates lipid degradation in a reversible pH-controlled manner (midpoint pH 5.3). Using negative and neutral vesicles and charge mutants, they concluded that the pH dependence is not a result of unfavorable interactions with charged headgroups but a result of a lack of favorable interactions with protein charges in the apolar fatty acid tail environment (*54*). Thus, two glutamate to glutamine mutations, eliminating two negatively charged groups result in a higher pH for the midpoint of the vesicle association. However, the stability to unfolding of the protein is also important (*55*). This probably explains why the Ca^{2+}-loaded state resists micelle association better despite the fact that it has a lower overall charge: the melting point increases as much as 35 °C upon Ca^{2+} binding.

Structure. The H^{α} chemical shifts show that the helices are largely preserved, in agreement with CD measurements, but that the β-type interactions are lost (Figure 7 and Table 1). The loss of β-type interactions suggests a general loss of native tertiary interactions and so does the negligible ring-current contribution from the aromatic ring of Y13 to the H^{α} chemical shift of L31 in the micelle-associated state. This contribution is conserved in the apo and Ca^{2+}-loaded states and shows how little the tertiary interactions vary with Ca^{2+} loading in EF-hand I. It is worth noting that in contrast to the study of Bcl x_L (*24*), the length of the helices in calbindin D_{9k} does not seem to change significantly upon micelle association.

The fact that most backbone H^N show NOEs to the DPC protons suggests that the entire protein is dissolved in the micelle (Figure 9). This observation is supported by the much lower number of NOEs to water. Large stretches including helix A and loop I and most of loop II appear to be without contact to water. This is a very interesting situation considering that the micelle is only twice the size of the protein (19 compared to 9 kD; Figure 1D), assuming the number of DPC molecules in the micelle does not change in the presence of the protein. It should be noted that the observed NOEs represent an average over many milliseconds and that all of these NOEs do not have to be fulfilled simultaneously. Interestingly, the NOEs between water and helix C agree well with its surface orientation (Figure 9) suggested from the hydrophobic moment. Helix C is clearly amphiphatic with a strong hydrophobic moment that is well-defined along the helix (data not shown). Although helices A, B, and D all show amphiphatic tendencies, their average per residue hydrophobic moments are much smaller and less well-defined.

Many studies have indicated that helix C is more loosely associated with the protein core than the other helices. In the structure of the apo protein, the orientation of helix C relative to the other helices is more uncertain (*22*); it has faster H^N exchange rates (*21*, *56*), and it has lower average H−N order parameters (*13*). Furthermore, in the apo state of the F36G mutant of calbindin D_{9k}, the deletion of an aromatic side chain at the end of helix B leaves EF-hand I mostly intact while entirely shifting the orientation of helix C (*57*). In the present study, the changes in H^N, N^H, and H^{α} chemical shifts (Table 1) are all lower in helix C than in the rest of the helices. An attractive explanation for the difference in chemical-shift changes is that when apo calbindin D_{9k} comes into contact with DPC micelles, helices A, B, and D are more perturbed by merging into the micelle, possibly because they form a more rigidly packed unit than helix C in the native state, while the clearly amphiphatic helix C is more independent of the specific environment. The resulting picture of the native protein includes helix A, B, and D and loop I as one unit, with helix C and loop II floating on top. This picture is in very good agreement with observations for many other S100 proteins, where the reorientation of helix C is by far the most significant structural change upon Ca^{2+} binding (*58*).

Dynamics. The transition between the micelle-free and micelle-associated states requires large conformational rearrangements. When apo calbindin D_{9k} associates with micelles, the exchange rate is of the order of $\sim$1000 s^{-1}, but the exchange rate with the Ca^{2+}-loaded state is $\sim$6 s^{-1}. Although the absence of exchange peaks for the residues in EF-hand II (Figure 10) seems to indicate an exchange rate that is too slow to produce exchange peaks, i.e., < 0.5 s^{-1}, it is more likely that the exchange peaks are absent because of an additional Ca^{2+} exchange phenomenon around loop II (Figure 10). The fact that micelle association occurs more readily and more than 100-fold faster with the apo protein shows that the bound Ca^{2+} ions have to dissociate before micelle association can occur and that Ca^{2+} dissociation is the rate-limiting step in micelle association from the Ca^{2+}-loaded state. In fact, the observed exchange rate for micelle association for the Ca^{2+}-saturated protein agrees well with Ca^{2+} off rates of 8.6 $\pm$ 1.5 and 48.0 $\pm$ 7.0 s^{-1}, obtained using stopped-flow measurements [100 mM KCl at 20 °C and pH 7.0 (*59*)].

The different exchange processes occurring in the two sites suggests that there is a difference in terms of the ability to bind Ca^{2+} when associated with the micelle, where micelle association seems to be intimately coupled to the loss of Ca^{2+} binding to EF-hand I, while EF-hand II may retain part of its Ca^{2+} affinity in the micelle-associated state. This suggests that loop I needs tertiary interactions to be able to form a Ca^{2+}-binding site, while loop II does not. The suggested localization of helix C on the surface might also be important in allowing Ca^{2+} binding to loop II.

The distinctive EF-hand I of calbindin D_{9k} is considerably more selective for Ca^{2+} than EF-hand II, the canonical EF-hand (*vide supra*) (*14*, *60*). The conformational changes to accommodate Ca^{2+} are also smaller in EF-hand I (*12*, *22*,

61). Also, Ca^{2+} induced the changes in the pico- to nanosecond dynamics of EF-hand I that are much smaller than those for EF-hand II (*13*, *16*). This feature appears to be a characteristic of the entire EF-hand (I) rather than of its Ca^{2+}-binding loop alone (*20*). The adaptivity of the regular EF-hand (II) is demonstrated by the X-ray structure of the $(Mg^{2+})_1$ state of calbindin D_{9k}, which shows that the smaller Mg^{2+} is accommodated in site II by translating helix C about 2 Å toward loop II compared to the apo and Ca^{2+}-loaded states (*14*). Remarkably, if indeed there is residual Ca^{2+} in EF-hand site (II) in the micelle-associated state, our notion of the adaptability of this site is extended significantly.

Biological Function. In this study, we have found clear evidence that the cytosolic protein calbindin D_{9k} interacts with DPC molecules and micelles. These results suggest the potential involvement of interactions with phospholipids and membranous material in the function of this protein in the cell.

A study of Chiba and Mohri (*7*) shows interesting resemblance with the present results. They found that a number of lysophospholipids had an enhancing effect on the fluorescence of DNS-labeled calbindin D_{9k}, suggesting a greater accessibility to the solvent for the DNS probe. The effect was only present in the absence of Ca^{2+} and only with lysophospholipids, which is interesting because DPC and lysophospholipids have the same headgroup. The lysophospholipids also protect calbindin D_{9k} from proteolytic digestion in the absence of Ca^{2+}. The authors suggested that the interaction was not dependent on micelle formation because effects were observed below the cmc. However, in the light of the uncertainty in the aggregation number in a protein-containing micelle (*vide supra*), we find it likely that this interaction indeed is analogous to the interaction with DPC micelles studied here. Most interestingly, one of the lysophospholipids, lyso-phosphatidylcholine (lyso-PC), constitutes 8.7% of the total phospholipid content in rat intestinal brush border membrane. Calbindin D_{9k} is also known to be present at very high levels in the lining of enterocytes (*vide infra*) (*62*).

Calbindin D_{9k} has a relatively high affinity for Ca^{2+} [$K_{d,mean}$ = 400 nM at 150 mM KCl, pH 7.5; (*19*)]. This is a critical property in its role in Ca^{2+} uptake, where it is essential to chelate Ca^{2+} at a level allowing for effective transport while at the same time maintaining Ca^{2+} homeostasis. The experiments reported here show that the interaction with phospholipids or phospholipid aggregates, such as the cell membrane, may have an impact on the Ca^{2+}-transport dynamics by calbindin D_{9k}. The interaction with DPC monomers in the Ca^{2+}-loaded state suggests that the Ca^{2+} affinity may be tuned by the concentration of small amphiphilic lipids and vice versa.

The low pH required for DPC micelle interactions to compete with Ca^{2+} binding to calbindin D_{9k} in our experiments is far below physiological pH, although significant variation in pH is well-known in certain cell compartments. Calbindin D_{9k} is strictly found inside epithelial cells of the small intestine and placenta and not exported to the rather acidic extracellular compartments of these organs. When it is exported into matrix vesicles in epiphyseal cartilage and bone (*6*), the pH of the surrounding cartilage fluids is around 7.6 (*63*). Micelle association competes with Ca^{2+} binding, which is strongest between pH 7 and 9 (*49*). At pH 5, where our measurements show about equal populations of the Ca^{2+}-loaded and the micelle-associated states, there is only a 30-fold attenuation of the Ca^{2+} affinity (low salt, 25 °C) (*49*). However, the equilibrium point depends on the numbers of Ca^{2+} and DPC−micelles available, and calbindin D_{9k} binding to DPC−micelle-like structures may well be competitive under a number of conditions. Furthermore, the interactions with DPC micelles presumably differ significantly from those with, e.g., the phospholipid membrane in a cell, which has a large surface area and where negatively charged headgroups give rise to a surface potential that lowers the local pH at the membrane surface significantly compared to the bulk pH (*64*, *65*).

In the enterocytes lining the brush border membrane, high levels of self-diffusing calbindin D_{9k} allow a higher *trans*-cellular Ca^{2+} flux while allowing the free Ca^{2+} levels in the cytoplasm to stay relatively low (*2*, *66*, *67*). One may speculate that if the apo state would have an affinity for the membranes in the cell it could, for example, make it easier for calbindin D_{9k} to give up the Ca^{2+} at the outlet. However, binding to the membrane at the outlet would impair diffusion of apo calbindin D_{9k} back to the inlet at the brush border membrane. On the other hand, if the affinity is significant only at the presumably more acidic brush border membrane, it would be expected to lead to higher local concentrations of both apo calbindin D_{9k} and Ca^{2+} at the inlet, which might have a positive impact on the Ca^{2+} dynamics. To judge the implications of calbindin D_{9k}−phospholipid interactions on *trans*-cellular Ca^{2+} flux, a new set of computer simulations such as those of Feher et al. (*67*) need to be made.

Our observations may also have implications for the function of the ancestral full-length S100 proteins. As discussed earlier, it is likely that many of the highly homologous S100 proteins interact with fatty acids and detergents in a manner similar to DPC and calbindin D_{9k}. Furthermore, they have a lower affinity for Ca^{2+} and a lower charge, making interactions with phospholipid aggregates more favorable and more competitive relative to Ca^{2+} binding.

Finally, the present data may also suggest a rather speculative mechanism for how S100B (*68*) and other S100 proteins could be secreted without a signal peptide. The potential association with the cell membrane may be a first step toward membrane passage in a way similar to antimicrobial peptides (*69*). The alternating affect of Ca^{2+} binding would then provide a means to regulate this function. The low ($\sim$100 μm) Ca^{2+} affinities of most of the S100 proteins would enable export from an intracellular compartment with less than 10 μM Ca^{2+} but not import from the extracellular milieu with 1 mM Ca^{2+}.

ACKNOWLEDGMENT

We thank Eva Thulin for protein expression and purification and Mikael Akke, Maria Håkansson, Sara Linse (Lund University), Charles Sanders (Vanderbilt University), and Howard Hsu (Kansas Medical Center) for helpful discussions.

REFERENCES

1. Kördel, J., Forsén, S., Drakenberg, T., and Chazin, W. J. (1990) The rate and structural consequences of proline cis−trans isomer-

ization in calbindin D_{9k}: NMR studies of the minor (*cis*-Pro43) isoform and the Pro43Gly mutant, *Biochemistry 29*, 4400−4409.
2. Bronner, F. (2003) Mechanisms of intestinal calcium absorption, *J. Cell. Biochem. 88*, 387−393.
3. Christakos, S., Gabrielides, C., and Rhoten, W. B. (1989) Vitamin D-dependent calcium-binding proteins: Chemistry, distribution, functional considerations, and molecular biology, *Endocr. Rev. 10*, 3−26.
4. Slepchenko, B. M., and Bronner, F. (2001) Modeling of transcellular Ca transport in rat duodenum points to coexistence of two mechanisms of apical entry, *Am. J. Physiol. Cell. Physiol. 281*, C270−C281.
5. Walters, J. R., Howard, A., Charpin, M. V., Gniecko, K. C., Brodin, P., Thulin, E., and Forsén, S. (1990) Stimulation of intestinal basolateral membrane calcium-pump activity by recombinant synthetic calbindin D_{9k} and specific mutants, *Biochem. Biophys. Res. Commun. 170*, 603−608.
6. Balmain, N. (1991) Calbindin-D9k. A vitamin-D-dependent, calcium-binding protein in mineralized tissues, *Clin. Orthop. 265*, 265−276.
7. Chiba, K., and Mohri, T. (1989) Conformation change of the intestinal calcium-binding protein induced by phospholipids in the presence and absence of Ca^{2+}, *Biochemistry 28*, 2995−2999.
8. Kretsinger, R. H., and Nockolds, C. B. (1973) Carp muscle calcium-binding protein, *J. Biol. Chem. 248*, 3313−3326.
9. Strynadka, N. C. J., and James, M. N. G. (1989) Crystal structures of the helix−loop−helix calcium-binding proteins, *Annu. Rev. Biochem. 58*, 951−998.
10. Schäfer, B. W., and Heizmann, C. W. (1996) The S100 family of calcium-binding proteins: Functions and pathology, *Trends Biochem. Sci. 21*, 134−140.
11. Vogel, H. J., Drakenberg, T., Forsén, S., O'Neil, J. D. J., and Hofmann, T. (1985) Structural difference in the two calcium binding sites of the porcine intestinal calcium binding protein: A multinuclear NMR study, *Biochemistry 24*, 3870−3876.
12. Akke, M., Forsén, S., and Chazin, W. J. (1995) Solution structure of $(Cd^{2+})_1$-calbindin D_{9k} reveals details of the stepwise structural changes along the apo, $(Ca^{2+})_1$, and $(Ca^{2+})_2$ binding pathway, *J. Mol. Biol. 252*, 102−121.
13. Akke, M., Skelton, N. J., Kördel, J., Palmer, A. G., and Chazin, W. J. (1993) Effects of ion binding on the backbone dynamics of calbindin D_{9k} determined by ^{15}N NMR relaxation, *Biochemistry 32*, 9832−9344.
14. Andersson, M., Malmendal, A., Linse, S., Ivarsson, I., Forsén, S., and Svensson, L. A. (1997) Structural basis for the negative allostery between Ca^{2+}- and Mg^{2+}-binding in the intracellular Ca^{2+}-receptor calbindin D_{9k}, *Protein Sci. 6*, 1139−1147.
15. Julenius, K., Thulin, E., Linse, S., and Finn, B. E. (1998) Hydrophobic core substitutions in calbindin D_{9k}: Effects on stability and structure, *Biochemistry 37*, 8915−8925.
16. Kördel, J., Skelton, N. J., Akke, M., Palmer, A. D., and Chazin, W. J. (1992) Backbone dynamics of calcium-loaded calbindin D_{9k} studied by two-dimensional proton-detected ^{15}N NMR spectroscopy, *Biochemistry 31*, 4856−4866.
17. Kragelund, B. B., Jönsson, M., Bifulco, G., Chazin, W. J., Nilsson, H., Finn, B. E., and Linse, S. (1998) Hydrophobic core substitutions in calbindin D_{9k}: Effects on Ca^{2+} binding and dissociation, *Biochemistry 37*, 8926−8937.
18. Linse, S., Brodin, P., Johansson, C., Thulin, E., Grundström, T., and Forsén, S. (1988) The role of protein surface charges in ion binding, *Nature 335*, 651−652.
19. Linse, S., Johansson, C., Brodin, P., Grundström, T., Drakenberg, T., and Forsén, S. (1991) Electrostatic contributions to the binding of Ca^{2+} in calbindin D_{9k}, *Biochemistry 30*, 154−162.
20. Malmendal, A., Carlström, C., Hambraeus, L., Drakenberg, T., Forsén, S., and Akke, M. (1998) Sequence and context dependence of EF-hand loop dynamics. An ^{15}N relaxation study of a calcium-binding site mutant of calbindin D_{9k}, *Biochemistry 37*, 2586−2595.
21. Skelton, N. J., Kördel, J., Akke, M., and Chazin, W. J. (1992) Nuclear magnetic resonance studies of the internal dynamics in apo, $(Cd^{2+})_1$, and $(Ca^{2+})_2$ calbindin D_{9k}. The rates of amide proton exchange with solvent, *J. Mol. Biol. 227*, 1100−1117.
22. Skelton, N. J., Kördel, J., and Chazin, W. J. (1995) Determination of the solution structure of apo calbindin D_{9k} by NMR spectroscopy, *J. Mol. Biol. 249*, 441−462.
23. Szebenyi, D. M. E., and Moffat, K. (1986) The refined structure of vitamin D-dependent calcium-binding protein from bovine intestine. Molecular details, ion binding, and implications for the structure of other calcium-binding proteins, *J. Biol. Chem. 261*, 8761−8777.
24. Losonczi, J. A., Olejniczak, E. T., Betz, S. F., Harlan, J. E., Mack, J., and Fesik, S. W. (2000) NMR studies of the anti-apoptotic protein Bcl-x_L in micelles, *Biochemistry 39*, 11024−11033.
25. Wang, J., Sahoo, D., Sykes, B. D., and Ryan, R. O. (1998) NMR evidence for a conformational adaptation of apolipophorin III upon lipid association, *Biochem. Cell. Biol. 76*, 276−283.
26. Johansson, C., Brodin, P., Grundström, T., Thulin, E., Forsén, S., and Drakenberg, T. (1990) Biophysical studies of engineered mutant proteins based on calbindin D_{9k} modified in the pseudo EF-hand, *Eur. J. Biochem. 187*, 455−460.
27. Thulin, E. (2002) Purification of recombinant calbindin D_{9k}, *Methods Mol. Biol. 172*, 175−184.
28. Zhang, O., Kay, L. E., Oliver, J. P., and Forman-Kay, J. D. (1994) Backbone ^1H and ^{15}N resonance assignments of the N-terminal SH3-domain of drk in folded and unfolded states using enhanced-sensitivity pulsed field gradient NMR techniques, *J. Biomol. NMR 4*, 845−858.
29. Montelione, G., and Wagner, G. (1989) 2D chemical exchange NMR spectroscopy by proton-detected heteronuclear correlation, *J. Am. Chem. Soc. 111*, 3096−3098.
30. Wider, G., Neri, D., and Wüthrich, K. (1991) Studies of slow conformational equilibria in macromolecules by exchange of heteronuclear longitudinal 2-spin-order in a 2D difference correlation experiment, *J. Biomol. NMR 1*, 93−98.
31. Bax, A., Ikura, M., Kay, L. E., Torchia, D. A., and Tschudin, R. (1990) Comparison of different modes of two-dimensional reverse-correlation NMR for the study of proteins, *J. Magn. Reson. 86*, 304−318.
32. Norwood, T. J., Boyd, J., Heritage, J. E., Soffe, N., and Cambell, I. D. (1990) Comparison of techniques for ^1H-detected heteronuclear ^1H-^{15}N spectroscopy, *J. Magn. Reson. 87*, 488−501.
33. Hartel, A. J., Lankhorst, P. P., and Altona, C. (1982) Thermodynamics of stacking and of self-association of the dinucleoside monophosphate m2(6)A-U from proton NMR chemical shifts: Differential concentration temperature profile method, *Eur. J. Biochem. 129*, 343−357.
34. Orbons, L. P., van der Marel, G. A., van Boom, J. H., and Altona, C. (1987) An NMR study of polymorphous behaviour of the mismatched DNA octamer d(m5C-G-m5C-G-A-G-m5C-G) in solution. The B-duplex and hairpin forms, *Eur. J. Biochem. 170*, 225−239.
35. Wishart, D. S., and Case, D. A. (2001) Use of chemical shifts in macromolecular structure determination, *Methods Enzymol. 338*, 3−34.
36. Delaglio, F., Grzesiek, S., Vuister, G. W., Zhu, G., Pfeifer, J., and Bax, A. (1995) NMRPipe: A multidimensional spectral processing system based on UNIX pipes, *J. Biomol. NMR 6*, 277−293.
37. Johnson, B. A., and Blevins, R. A. (1994) NMRVIEW−A computer program for the visualization and analysis of NMR data, *J. Biomol. NMR. 4*, 603−614.
38. Eisenberg, D., Schwarz, E., Komaromy, M., and Wall, R. (1984) Analysis of membrane and surface protein sequences with the hydrophobic moment plot, *J. Mol. Biol. 179*, 125−142.
39. Eisenberg, D., Weiss, R. M., and Terwilliger, T. C. (1984) The hydrophobic moment detects periodicity in protein hydrophobicity, *Proc. Natl. Acad. Sci. U.S.A. 81*, 140−144.
40. Engelman, D. M., Steitz, T. A., and Goldman, A. (1986) Identifying nonpolar transbilayer helices in amino acid sequences of membrane proteins, *Annu. Rev. Biophys. Biophys. Chem. 15*, 321−353.
41. Kördel, J., Forsén, S., and Chazin, W. J. (1989) ^1H NMR resonance assignments, secondary structure, and global fold in solution of the major (*trans*-Pro43) form of bovine calbindin D_{9k}, *Biochemistry 28*, 7065−7074.
42. Skelton, N. J., Akke, M., Kördel, J., Thulin, E., Forsén, S., and Chazin, W. J. (1992) ^{15}N NMR assignments and chemical shift analysis of uniformly labeled ^{15}N calbindin D_{9k} in the apo, $(Cd^{2+})_1$, and $(Ca^{2+})_2$ states, *FEBS Lett. 303*, 136−140.
43. Skelton, N. J., Forsen, S., and Chazin, W. J. (1990) ^1H NMR resonance assignments, secondary structure, and global fold of apo bovine calbindin D_{9k}, *Biochemistry 29*, 5752−5761.
44. Wishart, D. S., and Nip, A. M. (1998) Protein chemical shift analysis: A practical guide, *Biochem. Cell. Biol. 76*, 153−163.
45. Wishart, D. S., Sykes, B. D., and Richards, F. M. (1992) The chemical shift index−A fast and simple method for the assignment

of protein secondary structure through NMR spectroscopy, *Biochemistry 31*, 1647−1651.
46. McConnell, H. M. (1958) Reaction rates by nuclear magnetic resonance, *J. Chem. Phys. 28*, 430−431.
47. Palmer, A. G., III, Kroenke, C. D., and Loria, J. P. (2001) Nuclear magnetic resonance methods for quantifying microsecond-to-millisecond motions in biological macromolecules, *Methods Enzymol. 339*, 204−238.
48. Itou, H., Yao, M., Fujita, I., Watanabe, N., Suzuki, M., Nishihira, J., and Tanaka, I. (2002) The crystal structure of human MRP14 (S100A9), a Ca^{2+}-dependent regulator protein in inflammatory process, *J. Mol. Biol. 316*, 265−276.
49. Kesvatera, T., Jönsson, B., Telling, A., Tougu, V., Vija, H., Thulin, E., and Linse, S. (2001) Calbindin D(9k): A protein optimized for calcium binding at neutral pH, *Biochemistry 40*, 15334−15340.
50. Lauterwein, J., Bosch, C., Brown, L. R., and Wuthrich, K. (1979) Physicochemical studies of the protein−lipid interactions in melittin-containing micelles, *Biochim. Biophys. Acta 556*, 244−264.
51. Vinogradova, O., Sonnichsen, F., and Sanders, C. R., II (1998) On choosing a detergent for solution NMR studies of membrane proteins, *J. Biomol. NMR 11*, 381−386.
52. Cortese, J. D., Voglino, A. L., and Hackenbrock, C. R. (1998) Multiple conformations of physiological membrane-bound cytochrome *c*, *Biochemistry 37*, 6402−6409.
53. Dimitrova, M. N., Matsumura, H., Terezova, N., and Neytchev, V. (2002) Binding of globular proteins to membranes studied by isothermal titration calorimetry and fluorescence, *Colloids Surf., B 24*, 53−61.
54. de Alba, E., Weiler, S., and Tjandra, N. (2003) Solution structure of human saposin C: pH-dependent interaction with phospholipid vesicles, *Biochemistry 42*, 14729−14740.
55. Chakarova, S. D., and Carlsson, A. E. (2004) Model study of protein unfolding by interfaces, *Phys. Rev. E Stat. Phys., Plasmas, Fluids, Relat. Interdiscip. Top. 69*, 021907.
56. Linse, S., Teleman, O., and Drakenberg, T. (1990) Ca^{2+} binding to calbindin D_{9k} strongly affects the backbone dynamics: Measurements of exchange rates of individual amide protons using ^{1}H NMR, *Biochemistry 29*, 5925−5934.
57. Nelson, M. R., Thulin, E., Fagan, P. A., Forsén, S., and Chazin, W. J. (2002) The EF-hand domain: A globally cooperative structural unit, *Protein Sci. 11*, 198−205.
58. Bhattacharya, S., Bunick, C. G., and Chazin, W. J. (2004) Target selectivity in EF-hand calcium binding proteins, *Biochim. Biophys. Acta 1742*, 69−79.
59. Forsén, S., Linse, S., Thulin, E., Lindegård, B., Martin, S. R., Bayley, P. M., Brodin, P., and Grundström, T. (1988) Kinetics of calcium binding to calbindin mutants, *Eur. J. Biochem. 177*, 47−52.
60. Hofmann, T., Eng, S., Lilja, H., Drakenberg, T., Vogel, H. J., and Forsén, S. (1988) Site−site interactions in EF-hand calcium binding proteins, *Eur. J. Biochem. 172*, 307−313.
61. Skelton, N. J., Kördel, J., Akke, M., Forsén, S., and Chazin, W. J. (1994) Signal transduction versus buffering activity in Ca^{2+}-binding proteins, *Nat. Struct. Biol. 1*, 239−245.
62. Chapelle, S., and Gilles-Baillien, M. (1983) Phospholipids and cholesterol in brush border and basolateral membranes from rat intestinal mucosa, *Biochim. Biophys. Acta 753*, 269−271.
63. Howell, D., Pita, J., Marquez, J., and Madruga, J. (1968) Partition of calcium, phosphate, and protein in the fluid phase aspirated at calcifying sites in epiphyseal cartilage, *J. Clin. Invest. 47*, 1121−1132.
64. Eisenberg, M., Gresalfi, T., Riccio, T., and McLaughlin, S. (1979) Adsorption of monovalent cations to bilayer membranes containing negative phospholipids, *Biochemistry 18*, 5213−5223.
65. van der Goot, F. G., Gonzalez-Manas, J. M., Lakey, J. H., and Pattus, F. (1991) A "molten-globule" membrane-insertion intermediate of the pore-forming domain of colicin A, *Nature 354*, 408−410.
66. Bronner, F., Pansu, D., and Stein, W. D. (1986) An analysis of intestinal calcium transport across the rat intestine, *Am. J. Physiol. 250*, G561−G569.
67. Feher, J. J., Fullmer, C. S., and Wasserman, R. H. (1992) Role of facilitated diffusion of calcium by calbindin in intestinal calcium absorption, *Am. J. Physiol. 262*, C517−C526.
68. Barger, S. W., Wolchok, S. R., and van Eldik, L. J. (1992) Disulfide-linked S100 β dimers and signal transduction, *Biochim. Biophys. Acta 1160*, 105−112.
69. Zasloff, M. (2002) Antimicrobial peptides of multicellular organisms, *Nature 415*, 389−395.
70. Svensson, L. A., Thulin, E., and Forsén, S. (1992) Proline cis−trans isomers in calbindin D_{9k} observed by X-ray crystallography, *J. Mol. Biol. 223*, 601−606.
71. Tieleman, D. P., van der Spoel, D., and Berendsen, H. J. C. (2000) Molecular dynamics simulations of dodecylphosphocholine micelles at three different aggregate sizes: Micellar structure and chain relaxation, *J. Phys. Chem. B 104*, 6380−6388.
72. Koradi, R., Billeter, M., and Wütrich, K. (1996) MOLMOL: A program for display and analysis of macromolecular structures, *J. Mol. Graphics 14*, 51−55.

BI050088Z